Eur. Phys. J. C 30, 345–357 (2003)
Digital Object Identifier (DOI) 10.1140/epjc/s2003-01281-6

THE EUROPEAN PHYSICAL JOURNAL C

QCD corrections to electroweak vector boson scattering at small scattering angles

K. Peters[1,a], G.P. Vacca[2,b]

[1] II. Institut für Theoretische Physik, Universität Hamburg, Luruper Chaussee 149, 22761 Hamburg, Germany
[2] Dipartimento di Fisica - Università di Bologna and INFN – Sezione di Bologna, via Irnerio 46, 40126 Bologna, Italy

Received: 21 May 2003 /
Published online: 29 August 2003 –

Abstract. We investigate the role of a certain class of QCD corrections to electroweak vector boson scattering at small scattering angles and large energies. These are present since, from the perturbative analysis, the vector bosons may dissociate into quark–antiquark pairs giving rise to color dipoles interacting through gluon exchanges. After the computation of the vector boson impact factors, we present expressions for the lowest order QCD scattering amplitude and for the leading logarithmic BFKL amplitude. Particularly we discuss numerical results for the process $\gamma\gamma \to ZZ$. The QCD corrections to the cross section resulting from the interference with the electroweak ones are estimated and compared with the leading pure electroweak part. Corrections resulting from the leading log BFKL amplitude are of the order of a few percent already at the 0.5–1 TeV energy range.

1 Introduction

The search for physics beyond the standard model (SM) and the determination of the crucial and still not understood mechanism of the electroweak symmetry breaking in the SM itself are major subjects of investigation in particle physics. There is the hope to increase the understanding with the help of the next generation of supercolliders, and major efforts in this direction have currently been made. First insights are expected from the future Large Hadron Collider (LHC) runs. On the other hand high precision measurements at the Next Linear Collider (NLC) are considered to be of great importance, with features complementary to LHC. Next Linear Collider is a generic name for a e^+e^- machine operating in the energy regime up to 1 TeV, providing a very clean environment, and making available observables for many processes at an accuracy better than the percent level. In addition to the e^+e^- collider mode, one may have the capability of running the NLC in a $\gamma\gamma$ collision mode via Compton backscattering of laser photons off the linear collider electrons.

One of the important processes one may consider in a linear collider is the scattering of vector bosons. Indeed, at the NLC the electron and positron bunches can radiate vector bosons which interact thereafter. Various scenarios are considered also in the Compton collider mode. Each incoming photon may turn into a virtual WW pair, followed by the scattering of one W of each pair to end with WW or ZZ states [1]. There are also the processes where initial photons scatter directly into arbitrary vector bosons.

Vector boson scattering is related to the open question of mass generation. Since the longitudinal modes of the massive vector bosons reflect the nature of the Goldstone modes of the unbroken theory, these may give important information about the nature of electroweak symmetry breaking. Without the discovery of a scalar Higgs particle the vector bosons have to interact strongly at TeV scales, in order to preserve unitarity. In this scenario the vector boson scattering will be one of the key processes to be studied in the nearest future [2].

Another important question one may pose while searching for new physics is the existence of anomalous triple and quartic vector boson couplings which may affect vector boson scattering. Contact interactions are regarded as a possible extension of the SM, which can be well investigated with vector boson scattering [3]. The natural order of magnitude of the anomalous couplings [4] is small and, in order to eventually extract them, one needs to both measure and compute theoretically the SM cross sections with a precision better than 1%.

In this context the $\gamma\gamma \to ZZ$ process has a special role. Since there is no perturbative contribution at the tree level, such a process is sensitive to the particles and the new physics phenomena which contribute through radiative corrections [5]. This leads to an independent and complementary method to the direct production of new particles. In the same process the detection of CP violating phases [6] or additional effects due to the exchange of Kaluza–Klein gravitons in large extra-dimension scenarios [7] have been discussed.

[a] e-mail: krisztian.peters@desy.de
[b] e-mail: vacca@bo.infn.it

In summary, vector boson scattering processes may be seen as a central tool to probe physics beyond the SM and to reveal the nature of symmetry breaking. In order to exploit these features, a high precision is needed, both on the experimental and on the theoretical side. Calculations of these processes at the lowest available order may not be accurate enough. One loop corrections have been calculated for all those vector bosonic processes [8] where a tree level contribution is present. For the $\gamma\gamma \to ZZ$ process, which starts at one loop in α_{EW}, no higher order corrections are available yet. The question naturally arise, if this accuracy is high enough to disentangle new physics from the SM, providing a window to non-accessible energy regimes.

The aim of this paper is to address the question if the QCD corrections could play a role in vector boson scattering processes. Naively this seems not to be the case, since they arise only at higher loop corrections. On the other hand, even if the lowest order non-suppressed QCD correction to the amplitude for this process is smaller by $O(\alpha_{\mathrm{s}}^2)$ with respect to the electroweak one, in the cross section the interference among the two can reach the percent level. Moreover at high energies there are kinematical regimes wherein the emission of soft gluons generates large logs in the energy which make the QCD amplitude increasing with energy.

The electroweak cross section of $VV \to VV$ (with $V = W, Z, \gamma$) gains its biggest contribution from small scattering angles, and with increasing scattering energy the cross sections are approaching a constant in computations up to the one loop level. This contribution is coming from diagrams where only spin-1 particles are exchanged in the t-channel. At leading order and $O(\alpha_{\mathrm{EW}}^2)$ these exchanged particles are only electroweak vector bosons.

The same configuration arises for QCD corrections with gluons in the t-channel. The first gluonic contributions, which arise at the two loop level, are suppressed since these gluons are always accompanied by fermions in the t-channel. The non-suppressed QCD contributions occur at higher orders. These emerge when the vector bosons fluctuate into a quark–antiquark pair and these dipoles interact through gluons. At the lowest order, when two gluons are exchanged in the t-channel, one obtains a contribution constant in energy while higher order corrections provide large logarithms in the energy. These contributions cannot be neglected at large energies. The extreme attitude is to consider a resummation described by the BFKL equation [9] which gives an upper bound estimate of these effects.

We study in detail these QCD corrections for the reaction $\gamma\gamma \to ZZ$, whose cross section up to now was only studied at leading order (one loop in the electroweak sector) by Jikia [10]. His results show that the cross section is approaching a constant for high energies and its main contribution comes from the helicity conserving amplitudes at small scattering angles. This is exactly the kinematical region where the above discussed QCD contributions have their biggest influence.

We begin with the analytic calculations for an arbitrary bosonic process. In the Sect. 2 the two gluon exchange amplitude is computed, including the calculation of the non-forward impact factor. Since we consider the high-energy limit the amplitude factorize into two independent impact factors, built from the bosonic wave functions which describe the probability that a vector boson fluctuates into a quark–antiquark pair. In the Sect. 3 the cross section of the resummed gluonic contribution is presented, i.e. the BFKL amplitude. In order to give some numerical estimates, we concentrate on the definite process $\gamma\gamma \to ZZ$. In the Sect. 4 we calculate the EW and QCD parts of the amplitude in the Regge limit. Next we evaluate the corrections numerically. Because of the strong scale dependence we can give only estimates of the corrections, which we find to be of the order of a few percent. Finally we present our conclusions.

Our results suggest that, in particular in the small angle region, possible deviations from EW calculations cannot be interpreted as signals of new physics without taking into account the QCD corrections.

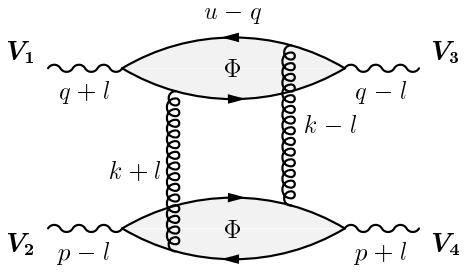

Fig. 1. The two gluon exchange of the $VV \to VV$ elastic cross section

2 Impact factors and lowest order QCD contribution

At high energies the lowest order leading QCD contribution to the vector boson scattering is pictured in Fig. 1, where the lowest order diagrams with two-gluon exchange are illustrated. The vector boson fluctuation into a quark–antiquark pair is described by the product of the two boson wave functions. This quantity is called the (non-forward) vector boson impact factor. Due to the high-energy factorization one can compute first the impact factors and then integrate these with the gluon propagators. In the high-energy limit, corresponding to s going to infinity and t fixed (Regge limit), we calculate first the s-channel discontinuity and restore after the amplitude through dispersion relations. Thus the intermediate quark lines inside the impact factors are taken on-shell. This procedure and the high-energy factorization simplifies the calculation significantly. The s-channel discontinuity of the scattering amplitude takes the form

$$\mathrm{Disc}_s A = \mathrm{i}s \int \frac{\mathrm{d}^2\mathbf{k}}{(2\pi)^3} \frac{\Phi(q,k,l)}{(\mathbf{k}+\mathbf{l})^2} \frac{\Phi(p,-k,-l)}{(\mathbf{k}-\mathbf{l})^2}\,, \qquad (1)$$

where Φ is the impact factor and the boldface marked letters are the transverse part of the Euclidean momenta. As

usual, the integration of the two longitudinal components of the loop momenta are absorbed into the definition of the impact factors. The remaining integrals may be computed numerically.

The momenta of the incoming bosons are $q+l$ and $p-l$, while the outgoing bosons have momenta $q-l$ and $p+l$. We use Sudakov variables with the light cone vectors $p' = p + yq'$, $y \simeq -p^2/2p'\cdot q'$ and $q' = q + xp'$, $x \simeq -q^2/2p'\cdot q'$, while $s = (p+q)^2 \simeq 2p'\cdot q'$ denotes as usual the squared center of mass energy of the VV scattering process. Then one parametrizes any 4-momentum u as

$$u = \alpha_u q' + \beta_u p' + u_\perp \,. \tag{2}$$

The impact factor for incoming and outgoing photons has been calculated recently [11] and since we adopt the momentum assignment which was given there, we refer the reader to this paper for further details of the calculation.

The incoming and outgoing bosons are characterized by the invariants $Q_+^2 = -(q+l)^2$, $Q_-^2 = -(q-l)^2$ and by similar expressions associated to the other two bosons involved in the process. For the full process the Mandelstam variable $t = (2l)^2$ has to be considered. In the case of on-shell bosons the virtuality reduces to the boson mass, i.e. $Q^2 = -M_V^2$.

We recall that in the limit of Regge kinematics one can neglect terms which are suppressed by powers of t/s and $Q_\pm^2/s$, leading to important simplifications. Let us consider the polarization vectors for the upper incoming and outgoing bosons. Their longitudinal polarization in terms of the Sudakov variables are given by

$$\epsilon_{\rm L}(q \pm l) \,=\, \frac{1}{|Q_\pm|}\left[(1 \pm \alpha_l)\, q' + \left(x \mp \beta_l - \frac{2l_\perp^2}{s}\right) p' \pm l_\perp\right], \tag{3}$$

while the transverse polarization vectors are

$$\epsilon_{\rm T}^{(h)}(q \pm l) \,=\, \epsilon_\perp^{(h)} \,\pm\, \frac{2l_\perp \cdot \epsilon_\perp^{(h)}}{s}\,(q' - p' \pm l_\perp)\,, \tag{4}$$

where $h = \pm$ denotes two helicity states and

$$\epsilon_\perp^{(h)} \,=\, \frac{1}{\sqrt{2}}\,(0, 1, \pm {\rm i}, 0)\,. \tag{5}$$

Again, for the bosons appearing in the lower impact factor the same expression holds with an exchange of q and p and $l \to -l$.

A difference between the photon and the other bosons is given by the chiral coupling to the quarks of the latter ones. Consequently extra terms in the traces appear and the ones proportional to odd powers of γ^5 do not contribute because of charge conjugation invariance. Thus, regarding the impact factors, the W and Z bosons behave both in the same way as the photon, i.e. we can use the result from [11], and only the magnitude of the coupling to the quarks depends on the nature of the boson.

The impact factor where both of the bosons have longitudinal polarizations takes the form

$$\begin{aligned}
&\Phi_{\rm LL}(q,k,l) \qquad\qquad (6)\\
&= \alpha_{\rm s}\sqrt{N_c^2-1}\sum_f C_f\, 4\sqrt{4\pi}\,|Q_+||Q_-|\int_0^1 {\rm d}\alpha \int \frac{{\rm d}^2\mathbf{u}}{(2\pi)^2}\\
&\quad\times\alpha^2(1-\alpha)^2\left(\frac{1}{D_1^+}-\frac{1}{D_2^+}\right)\left(\frac{1}{D_1^-}-\frac{1}{D_2^-}\right),
\end{aligned}$$

while for transverse polarized bosons we have

$$\begin{aligned}
&\Phi_{TT}^{(ij)}(q,k,l) \qquad\qquad (7)\\
&= \alpha_{\rm s}\,\sqrt{N_c^2-1}\sum_f C_f\,\sqrt{4\pi}\int_0^1 {\rm d}\alpha\int\frac{{\rm d}^2\mathbf{u}}{(2\pi)^2}\\
&\times\left\{-4\alpha(1-\alpha)\;\boldsymbol{\epsilon}_i\cdot\left(\frac{\mathbf{N}_1^+}{D_1^+}-\frac{\mathbf{N}_2^+}{D_2^+}\right)\left(\frac{\mathbf{N}_1^-}{D_1^-}-\frac{\mathbf{N}_2^-}{D_2^-}\right)\cdot\boldsymbol{\epsilon}_j^*\right.\\
&+\boldsymbol{\epsilon}_i\cdot\boldsymbol{\epsilon}_j^*\left[\left(\frac{\mathbf{N}_1^+}{D_1^+}-\frac{\mathbf{N}_2^+}{D_2^+}\right)\cdot\left(\frac{\mathbf{N}_1^-}{D_1^-}-\frac{\mathbf{N}_2^-}{D_2^-}\right)\right.\\
&\left.\left.+\;m_f^2\left(\frac{1}{D_1^+}-\frac{1}{D_2^+}\right)\left(\frac{1}{D_1^-}-\frac{1}{D_2^-}\right)\right]\right\}.
\end{aligned}$$

Finally, if the incoming boson is transverse polarized while the outgoing one is longitudinal, the impact factor reads

$$\begin{aligned}
&\Phi_{\rm LT}^{(j)}(q,k,l) \qquad\qquad (8)\\
&= \alpha_{\rm s}\sqrt{N_c^2-1}\sum_f C_f\,2\sqrt{4\pi}\,|Q_+|\int_0^1{\rm d}\alpha\int\frac{{\rm d}^2\mathbf{u}}{(2\pi)^2}\\
&\times\,\alpha(1-\alpha)(1-2\alpha)\left(\frac{1}{D_1^+}-\frac{1}{D_2^+}\right)\left(\frac{\mathbf{N}_1^-}{D_1^-}-\frac{\mathbf{N}_2^-}{D_2^-}\right)\cdot\epsilon_i^*\,,
\end{aligned}$$

and vice versa for the incoming boson longitudinal and the outgoing one transverse, one has

$$\begin{aligned}
&\Phi_{\rm TL}^{(i)}(q,k,l) \qquad\qquad (9)\\
&= \alpha_{\rm s}\sqrt{N_c^2-1}\sum_f C_f\,2\sqrt{4\pi}\,|Q_-|\int_0^1{\rm d}\alpha\int\frac{{\rm d}^2\mathbf{u}}{(2\pi)^2}\\
&\times\;\alpha(1-\alpha)(1-2\alpha)\;\epsilon_i\cdot\left(\frac{\mathbf{N}_1^+}{D_1^+}-\frac{\mathbf{N}_2^+}{D_2^+}\right)\left(\frac{1}{D_1^-}-\frac{1}{D_2^-}\right),
\end{aligned}$$

where $\boldsymbol{\epsilon}_j = 1/\sqrt{2}(1,\pm{\rm i})$ are two-dimensional polarization vectors corresponding to the two transverse polarizations $j = \pm$. We have also used

$$\begin{aligned}
D_1^\pm &= (\mathbf{u} \pm (1-\alpha)\mathbf{l})^2 \,+\, \alpha(1-\alpha)\,Q_\pm^2 \,+\, m_f^2\,,\\
D_2^\pm &= (\mathbf{u} - \mathbf{k} \mp \alpha\mathbf{l})^2 \,+\, \alpha(1-\alpha)\,Q_\pm^2 \,+\, m_f^2\,,\\
\mathbf{N}_1^\pm &= \mathbf{u} \pm (1-\alpha)\mathbf{l}\,,\\
\mathbf{N}_2^\pm &= \mathbf{u} - \mathbf{k} \mp \alpha\mathbf{l}\,.
\end{aligned} \tag{10}$$

Marked in boldface are the Euclidean form of the transverse momenta, i.e. $u_\perp^2 = -\mathbf{u}^2 < 0$. The constant C_f is the product of the coupling of the incoming and outgoing boson to the quarks of flavor f. The impact factors have been written in a factorized form where the two parts correspond to the boson wave functions, describing the probability that a boson dissociates into a quark–antiquark

pair. In order to obtain the lowest order QCD amplitude, one has to substitute these impact factors into (1) and integrate over the gluon momenta.

The two helicity-flip impact factors are in general non-zero. They vanish only for forward scattering, where $\mathbf{l} = 0$. This is due to the different symmetry behavior of the transverse and longitudinal boson wave functions. This property is more trasparent in the coordinate space formulation, (34) of [11]. Here the impact factor is written as a convolution of the two boson wave functions and the dipol interaction. The dipole interaction is invariant under the transformation of the dipole size vector $\mathbf{r} \to -\mathbf{r}$, and so is the longitudinal wave function, (22) of [11]. In contrast to this the transverse wave function, (28)–(31) of [11], is antisymmetric under this transformation, since it is proportional to $\mathbf{r}$. The convolution of two transverse wave functions is therefore symmetric under this transformation, whereas the convolution of a transverse and a longitudinal one is antisymmetric, leading to the vanishing result for $\mathbf{l} = 0$. If $\mathbf{l}$ is non-zero, these symmetry properties are broken, resulting in a non-vanishing Φ_{TL} and Φ_{TL}.

3 Leading log (BFKL) contribution

At high energies and close to the forward region (Regge limit), higher order contributions in α_{s} start to be important. Diagrams of ladder topology, built with (non-elementary) reggeized gluons, can contribute up to the order $\alpha_{\mathrm{s}}^n \ln^n(s/s_0)$. On retaining the leading logarithmic (LL) contributions and performing a resummation a rough estimate (overestimate) of the total QCD corrections is obtained. Nonetheless one expects to find the QCD contribution to the process in the window constrained by the simple two gluon exchange on one side and the resummed LL BFKL pomeron exchange on the other.

This possibility is related to the property of the factorization of the QCD scattering amplitude, in the Regge limit, in terms of the impact factors associated to the external particles and the BFKL Green's function, as illustrated in Fig. 2.

For the physical process we want to study the impact factors have been calculated in the preceding section and the discontinuity of the LL resummed amplitude is simply obtained by inserting the non-forward BFKL pomeron Green's function in the place of the two gluon propagators. Indeed one has

$$\mathrm{Disc}_s A = \mathrm{i}s \int \frac{\mathrm{d}^2\boldsymbol{k}}{(2\pi)^3} \frac{\mathrm{d}^2\boldsymbol{k}'}{(2\pi)^3} \tag{11}$$
$$\times\, \Phi(q,k,l) G(y|\boldsymbol{k}+\boldsymbol{l}, \boldsymbol{k}-\boldsymbol{l}; \boldsymbol{k}'+\boldsymbol{l}, \boldsymbol{k}'-\boldsymbol{l}) \Phi(p,-k',-l),$$

where $y = \ln s/s_0$ is the rapidity variable and s_0 is a typical scale in the process. Clearly, for $\alpha_{\mathrm{s}} \to 0$, when all rungs of the BFKL resummation decouple, the Green's function reduces to describing the two gluon exchange, which means that we use the following normalization:

$$\lim_{\alpha_{\mathrm{s}}\to 0} G(y|\boldsymbol{k}+\boldsymbol{l}, \boldsymbol{k}-\boldsymbol{l}; \boldsymbol{k}'+\boldsymbol{l}, \boldsymbol{k}'-\boldsymbol{l})$$

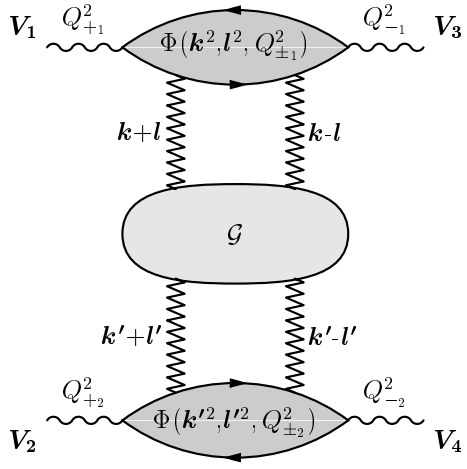

Fig. 2. The BFKL pomeron exchange in the $VV \to VV$ elastic cross section

$$= \frac{(2\pi)^3}{(\boldsymbol{k}+\boldsymbol{l})^2(\boldsymbol{k}-\boldsymbol{l})^2} \delta^{(2)}(\boldsymbol{k}-\boldsymbol{k}'). \tag{12}$$

In the following we briefly give the ingredients needed to construct the BFKL Green's function. The eigenfunctions $E_{h,\bar{h}}$ of the BFKL kernel, which appears in the integral Bethe–Salpeter-like equation resumming all the LL terms, are well known in coordinate space, wherein their form is dictated by conformal invariance. They are given by

$$E_{h,\bar{h}}(\boldsymbol{r}_{10}, \boldsymbol{r}_{20}) = \left(\frac{r_{12}}{r_{10} r_{20}}\right)^h \left(\frac{r^*_{12}}{r^*_{10} r^*_{20}}\right)^{\bar{h}}, \tag{13}$$

with $\boldsymbol{r}_{ij} = \boldsymbol{r}_i - \boldsymbol{r}_j$ etc., $h = (1+n)/2 + \mathrm{i}\nu$, $\bar{h} = (1-n)/2 + \mathrm{i}\nu$ ($h^* = 1-\bar{h}$, $\bar{h}^* = 1-h$). Let us note that standard complex notation for two-dimensional vectors is used on the right-hand side. The conformal weights h, decomposed in n (integer conformal spin) and ν (real), label the principal series of unitary representations of the Möbius group. Fourier transforming to momentum space (we use the Lipatov's convention which assigns a $1/(2\pi)^2$ to any coordinate integration) one finds [15]:

$$\tilde{E}_{h\bar{h}}(\boldsymbol{k}_1, \boldsymbol{k}_2) = \int \frac{\mathrm{d}^2\boldsymbol{r}_1}{(2\pi)^2} \frac{\mathrm{d}^2\boldsymbol{r}_2}{(2\pi)^2} E_{h,\bar{h}}(\boldsymbol{r}_1, \boldsymbol{r}_2) e^{\mathrm{i}(\boldsymbol{k}_1\cdot\boldsymbol{r}_1 + \boldsymbol{k}_2\cdot\boldsymbol{r}_2)}$$
$$= C\Big(X(\boldsymbol{k}_1, \boldsymbol{k}_2) + (-1)^n X(\boldsymbol{k}_2, \boldsymbol{k}_1)\Big). \tag{14}$$

The coefficient C is given by

$$C = \frac{(-\mathrm{i})^n}{(4\pi)^2} h\bar{h}(1-h)(1-\bar{h}) \Gamma(1-h)\Gamma(1-\bar{h}). \tag{15}$$

The functions X in complex notation can be expressed in terms of hypergeometric functions:

$$X(\boldsymbol{k}_1, \boldsymbol{k}_2) = \left(\frac{k_1}{2}\right)^{\bar{h}-2} \left(\frac{k_2^*}{2}\right)^{h-2} \tag{16}$$
$$\times\, F\left(1-h, 2-h; 2; -\frac{k_1^*}{k_2^*}\right) F\left(1-\bar{h}, 2-\bar{h}; 2; -\frac{k_2}{k_1}\right).$$

This analytic form does not contain any term of the type $\delta^2(\boldsymbol{k}_1)$ or $\delta^2(\boldsymbol{k}_2)$ which are present in the coordinate representation (13). The impact factor of a colorless external particle vanishes for zero momentum of any gluon exchanged and therefore the delta-function type terms do not contribute.

The pomeron intercept has the form $\alpha_{\rm P}(0) = 1 + \chi(\nu, n)$, where

$$\chi(\nu,n) = \chi_h = \bar{\alpha}_{\rm s}\left(2\psi(1) - \psi\left(\frac{1+|n|}{2} + {\rm i}\nu\right) - \psi\left(\frac{1+|n|}{2} - {\rm i}\nu\right)\right), \qquad \bar{\alpha}_{\rm s} = \frac{N_c\alpha_{\rm s}}{\pi}, \tag{17}$$

are the kernel eigenvalues corresponding to the eigenfunctions in (13) and (14). We shall use the pomeron Green's function in the momentum representation. Starting from the form in coordinate representation [16] one can perform a Fourier transform [15] and making use of the Casimir operator properties of the Möbius group, one finally obtains [17] for the non-amputated Green's function

$$\begin{aligned}&\tilde{G}_2(y|\boldsymbol{k}_1,\boldsymbol{k}_2;\boldsymbol{k}_{1'}\boldsymbol{k}_{2'}) \\ &= (2\pi)^3\int {\rm d}\mu(h)\,{\rm e}^{y\,\chi_h}\,N_h(2\pi)^2 \\ &\quad\times\tilde{E}_{h,\bar{h}}(\boldsymbol{k}_1,\boldsymbol{k}_2)\tilde{E}^*_{h,\bar{h}}(\boldsymbol{k}_{1'},\boldsymbol{k}_{2'})\,,\end{aligned} \tag{18}$$

where we use the measure in the conformal weight space $\int {\rm d}\mu(h) = \sum_n \int {\rm d}\nu$ with the following normalization factor N_h:

$$N_h = \frac{(\nu^2+n^2/4)}{[\nu^2+(n-1)^2/4][\nu^2+(n+1)^2/4]}. \tag{19}$$

The $(2\pi)^3$ factor in front of the integral comes from the normalization fixed by (12).

Let us finally rewrite the expression of the amplitude discontinuity in (11) by inserting in it the relation (18). On defining the conformal weight representation for the impact factors according to

$$\Phi_h(q,l) = \int \frac{{\rm d}^2\boldsymbol{k}}{(2\pi)^3}\Phi(q,k,l)\tilde{E}_{h,\bar{h}}(\boldsymbol{k}+\boldsymbol{l},\boldsymbol{k}-\boldsymbol{l})\,, \tag{20}$$

together with the primed $\Phi'_h(q,l)$ computed with the conjugate eigenstate, one has

$${\rm Disc}_s A = {\rm i}s(2\pi)^5\int {\rm d}\mu(h)\,N_h\,{\rm e}^{y\,\chi_h}\,\Phi_h(q,l)\Phi'_h(p,l)\,. \tag{21}$$

We stress that due to high-energy factorization the energy dependence is encoded in the LL BFKL Green's function and the only other dependence in the momenta of the incoming particles is through the invariant external masses on which the impact factors depend. In the last expression the dominant contribution for large y can be easily extracted with a saddle point analysis for $n = 0$ around $\nu = 0$ and therefore reduces to

$${\rm Disc}_s A = {\rm i}s(2\pi)^5 16{\rm e}^{y\,\chi_0}\frac{\sqrt{2\pi}}{(2ay)^{3/2}}\Phi_0(q,l)\Phi'_0(p,l)\,, \tag{22}$$

where $\chi_0 = 4\ln(2)\bar{\alpha}_{\rm s}$ is the leading BFKL intercept and $a = 14\zeta(3)\bar{\alpha}_{\rm s}$.

The forward limit presents a well known cusp behavior and it must converge to the result obtained on using a forward BFKL Green's function,

$$G_{\rm F}(y|\boldsymbol{k},\boldsymbol{k}') = (2\pi)^3\int {\rm d}\mu(h)\,{\rm e}^{y\,\chi_h}\tilde{E}^{({\rm F})}_{h,\bar{h}}(\boldsymbol{k})\tilde{E}^{({\rm F})*}_{h,\bar{h}}(\boldsymbol{k}')\,, \tag{23}$$

which is written in the spectral represention with the forward BFKL amputated eigenfunctions given by $\tilde{E}^{({\rm F})}_{h,\bar{h}}(\boldsymbol{k}) = 1/(\pi\sqrt{2})k^{h-1}k^{*\,\bar{h}-1}$.

The saddle point approximations can be carried on in a way similar to the non-forward case. We shall define

$$\Phi^{({\rm F})}_h(q) = \int \frac{{\rm d}^2\boldsymbol{k}}{(2\pi)^3}\Phi(q,k,0)\frac{1}{\boldsymbol{k}^2}\tilde{E}^{({\rm F})}_{h,\bar{h}}(\boldsymbol{k})\,, \tag{24}$$

as well as a $\Phi^{'(F)}_h(q)$ for the scalar product with the conjugate pomeron state and write the discontinuity in the forward case as

$${\rm Disc}^{({\rm F})}_s A = {\rm i}s(2\pi)^3{\rm e}^{y\,\chi_0}\frac{\sqrt{2\pi}}{(2ay)^{1/2}}\Phi^{({\rm F})}_0(q)\Phi^{'(F)}_0(p)\,. \tag{25}$$

Let us note that in the transition from the non-forward to forward physics the perturbative QCD analysis is increasingly affected by the long distance interactions (contributions for all values of the impact parameter), since gluons are massless. This implies that some care is required to treat the general non-forward expression in this limit. The saddle point approximation for $n = 0$ around $\nu = 0$ leading to (22) is accurate only for l down to values of the order of one. Strictly speaking, performing the saddle point approximation of (21) in the region of very small l one needs to shift the saddle point which becomes l dependent. In our numerical calculation we have used (22) down to $|2\boldsymbol{l}|^2 = 1/2\,M_Z^2$, and then we have extrapolated to the forward value, (25).

A more precise analysis, avoiding the use of the saddle point approximation is of course possible but it is not needed for the order of magnitude estimate which is pursued here. By the way, few checks have been done with an exact Green's function computation, confirming such an expectation.

Finally, in order to evaluate the elastic cross sections we need to obtain the amplitude from the computed discontinuity. Instead of using the full dispersion relation technique, a simple evaluation compatible with the approximation adopted is given by

$$A \sim \left(1 - {\rm i}\frac{\pi}{2}\frac{\partial}{\partial y}\right)\frac{1}{2}{\rm Disc}_s A\,, \tag{26}$$

as provided by the signature factor in the partial wave amplitude analysis.

4 The process $\gamma\gamma \to ZZ$ in the small angle limit

We shall henceforth concentrate on a definite process, $\gamma\gamma \to ZZ$, and compute for it a numerical estimate of the QCD contributions. We recall that we are interested in the kinematical region of small scattering angles, i.e. scattering close to the forward region, so that one can do the calculation in the high-energy approximation suited for the Regge limit: terms which are suppressed by powers of t/s can be neglected, with a significant simplification in the computation. We shall, in fact, use the results presented in Sect. 2 and 3.

4.1 The leading electroweak contribution

Let us first analyze the pure electroweak contributions to the process. This process starts at one loop and was calculated by Jikia [10]. In order to calculate the QCD corrections to $\gamma\gamma \to ZZ$ one has to know the leading electroweak contribution at the amplitude level, add to it the leading QCD amplitude and take the modulus squared. The main contribution to the corrections will come from the interference term. In the high-energy limit where t is kept fixed most of the contributions are suppressed by powers of s. The surviving graphs are pictured in Fig. 3. Also for these only the helicity conserving amplitudes survive, with both of the bosons transverse polarized. One may confirm this by taking the limit s to infinity and keeping t fixed within the expressions of [10].

In order to simplify the calculation we compute first the s-channel discontinuity, i.e. the s-channel internal W lines are taken on-shell. Here the s-channel discontinuity coincides with twice the imaginary part of the amplitude. With the same assignment of the momenta already used in the last sections the imaginary part of the box contribution reads

$$\begin{aligned}&\operatorname{Im} A^{(1)}_{\gamma\gamma\to ZZ}\\ &= \frac{1}{2}\int \frac{\mathrm{d}^4k}{(2\pi)^2}\,\delta[(q-k)^2 - M_W^2]\;\delta[(p+k)^2 - M_W^2]\\ &\quad \times A^{(0)}_{\gamma\gamma\to WW} A^{(0)\dagger}_{WW\to ZZ}\,,\end{aligned} \tag{27}$$

where a summation over the W boson helicities is implied. Performing the loop integration and retaining only the leading power of s we get

$$\begin{aligned}\operatorname{Im} A_{\mathrm{Box}} &= s\,\alpha_{\mathrm{em}}^2\,\frac{c_{\mathrm{W}}^2}{s_{\mathrm{W}}^2}\,\frac{8\pi}{\sqrt{t^2-4tM_W^2}}\\ &\quad\times \ln\left[\left(\frac{-t+\sqrt{t^2-4tM_W^2}}{-t-\sqrt{t^2-4tM_W^2}}\right)^2\right],\end{aligned} \tag{28}$$

where $|2\mathbf{l}|^2 \approx -t$ was used. Equation (28) yields immediately the real part by just noting that $\ln(-s) = \ln s - \mathrm{i}\pi$. Thus the reconstructed (leading) full box amplitude reads

$$A_{\mathrm{Box}} = \frac{-s}{\pi}\ln\left(\frac{s}{t}\right)\,\alpha_{\mathrm{em}}^2\,\frac{c_{\mathrm{W}}^2}{s_{\mathrm{W}}^2}\,\frac{8\pi}{\sqrt{t^2-4tM_W^2}}$$

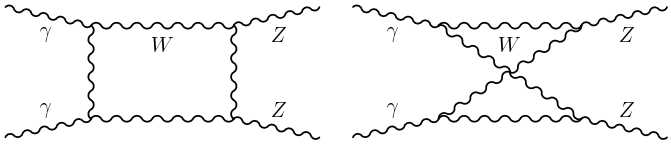

Fig. 3. The surviving contributions to the leading electroweak amplitude in the Regge limit for real γ and transverse polarized Z

$$\times \ln\left[\left(\frac{-t+\sqrt{t^2-4tM_W^2}}{-t-\sqrt{t^2-4tM_W^2}}\right)^2\right]. \tag{29}$$

The amplitude of the crossed diagram is obtained from the box contribution (29) by replacing s by $u \approx -s$. Adding the box and crossed contributions, at the end one is left with the imaginary part of the box diagram:

$$A^{++++}_{\mathrm{EW}} = A^{+-+-}_{\mathrm{EW}} = \mathrm{i}\,\operatorname{Im} A_{\mathrm{Box}} \tag{30}$$

Thus in the Regge limit the leading order electroweak contribution is purely imaginary ($s \gg -t$), and the cross section is constant in s. Considering the limiting behavior of (30) in the region $s \gg -t \gg M_W^2$ and for the case $t = 0$ one obtains the expressions presented in [10].

4.2 QCD corrections

The amplitude of this process in the high-energy limit is illustrated in Fig. 2. The ingredients needed have been discussed in Sects. 2 and 3. To proceed with an explicit calculation we have to specify the couplings C_f, which depend on the external bosons, and the virtualities appearing in the impact factors given in (7) and (9). The starting expressions are for massive quarks. For practical purposes only the top quark mass has to be taken into account because of the large Z mass. The integrals which correspond to the quark loop have to be performed. The last integration we compute is the scalar product of the impact factors with the BFKL states (20) and (24).

We calculate this process for all external bosons on-shell. In such a case we have Q_+^2 identically zero and $Q_-^2 = -M_Z^2$. The coupling constants C_f – the product of the γ-quark and Z-quark couplings – are given by

$$C_f = \frac{4\pi\alpha_{\mathrm{em}}}{2\sin\theta_{\mathrm{W}}\cos\theta_{\mathrm{W}}}\left\{q_f T_f^3 - 2\,q_f^2\sin^2\theta_{\mathrm{W}}\right\}. \tag{31}$$

First we consider the scattering of the photons into transverse Z bosons. To proceed we have to solve the remaining integrations for the impact factor Φ_{TT} in (7). In order to compute the integral over the two-dimensional Euclidean vector $\mathbf{u}$ we employ a standard Feynman parametrization and rewrite (7) as

$$\begin{aligned}&\Phi^{(ij)}_{\mathrm{TT}}(q,k,l)\\ &= \alpha_{\mathrm{s}}\sqrt{N_c^2-1}\sum_f C_f\sqrt{4\pi}\int_0^1 \mathrm{d}\alpha\int\frac{\mathrm{d}^2\mathbf{u}}{(2\pi)^2}\int_0^1 \mathrm{d}x\end{aligned}$$

$$\times \left\{ \frac{4\alpha(1-\alpha)[\boldsymbol{\epsilon}_i\cdot\mathbf{u}\;\boldsymbol{\epsilon}_j^*\cdot\mathbf{u} - x(1-x)\boldsymbol{\epsilon}_i\cdot\mathbf{p}_a\;\boldsymbol{\epsilon}_j^*\cdot\mathbf{p}_a]}{[u^2+x(1-x)p_a^2-xm+m_f^2]^2} \right.$$
$$- \frac{(u^2-x(1-x)p_a^2+m_f^2)(\boldsymbol{\epsilon}_i\cdot\boldsymbol{\epsilon}_j^*)}{[u^2+x(1-x)p_a^2-xm+m_f^2]^2}$$
$$- \frac{4\alpha(1-\alpha)[\boldsymbol{\epsilon}_i\cdot\mathbf{u}\;\boldsymbol{\epsilon}_j^*\cdot\mathbf{u} - x(1-x)\boldsymbol{\epsilon}_i\cdot\mathbf{p}_b\;\boldsymbol{\epsilon}_j^*\cdot\mathbf{p}_b]}{[u^2+x(1-x)p_b^2-xm+m_f^2]^2}$$
$$\left. - \frac{(u^2-x(1-x)p_b^2+m_f^2)(\boldsymbol{\epsilon}_i\cdot\boldsymbol{\epsilon}_j^*)}{[u^2+x(1-x)p_b^2-xm+m_f^2]^2} \right\}. \quad (32)$$

Here we have defined $\mathbf{p}_a = -\mathbf{k} - (1-2\alpha)\mathbf{l}$, $\mathbf{p}_b = 2\alpha\mathbf{l}$ and $m = \alpha(1-\alpha)(M_Z^2 + \mathrm{i}\epsilon)$. Strictly speaking, at this stage of the calculation m is taken negative and subsequently, after having performed the integrations, analytically continued to positive values obtaining the above definition. The first fraction corresponds to the two diagrams where one of the gluons is attached to the quark and the other to the antiquark. The second fraction corresponds to the two diagrams where the two gluons are attached to the same (anti)quark. Each of them would lead to a divergent integral but, or course, the sum in (32) gives a finite result.

On performing the $\mathbf{u}$ integration we end up with

$$\Phi_{\mathrm{TT}}^{(ij)}(q,k,l)$$
$$= \alpha_{\mathrm{s}}\sqrt{N_c^2-1}\sum_f C_f\sqrt{4\pi}\int_0^1\frac{\mathrm{d}\alpha}{2\pi}\int_0^1\mathrm{d}x$$
$$\times\left\{ -4\alpha(1-\alpha)\,x(1-x) \right. \quad (33)$$
$$\times\left(\frac{\boldsymbol{\epsilon}_i\cdot\mathbf{p}_a\;\boldsymbol{\epsilon}_j^*\cdot\mathbf{p}_a}{x(1-x)p_a^2-xm+m_f^2} - \frac{\boldsymbol{\epsilon}_i\cdot\mathbf{p}_b\;\boldsymbol{\epsilon}_j^*\cdot\mathbf{p}_b}{x(1-x)p_b^2-xm+m_f^2}\right)$$
$$+\,\boldsymbol{\epsilon}_i\cdot\boldsymbol{\epsilon}_j^*\left([\alpha^2+(1-\alpha)^2]\ln\left[\frac{x(1-x)p_a^2-xm+m_f^2}{x(1-x)p_b^2-xm+m_f^2}\right]\right.$$
$$\left.\left. +\;\frac{x(1-x)p_a^2-m_f^2}{x(1-x)p_a^2-xm+m_f^2} - \frac{x(1-x)p_b^2-m_f^2}{x(1-x)p_b^2-xm+m_f^2}\right)\right\}.$$

The computation of the x integration is straightforward. Due to the length of the result we present here only the limit $m_f \to 0$ which preserves a significant simplification compared to the massive case. The corresponding helicity conserving result with massive fermions is presented in the appendix. After the integration in the Feynman parameter variable, one obtains in the zero quark mass limit for the separate helicity states

$$\Phi_{\mathrm{TT}}^{(++)}(q,k,l) = \alpha_{\mathrm{s}}\sqrt{N_c^2-1}\sum_f C_f\sqrt{4\pi}\int_0^1\frac{\mathrm{d}\alpha}{2\pi}$$
$$\times\,[\alpha^2+(1-\alpha)^2]\;\ln\left[\frac{p_a^2-m}{p_b^2-m}\right] \quad (34)$$
$$\Phi_{\mathrm{TT}}^{(--)}(q,k,l) = \Phi_{\mathrm{TT}}^{(++)}(q,k,l) \quad (35)$$
$$\Phi_{\mathrm{TT}}^{(+-)}(q,k,l)$$
$$= \mathrm{i}\,\alpha_{\mathrm{s}}\sqrt{N_c^2-1}\sum_f C_f\sqrt{4\pi}\int_0^1\frac{\mathrm{d}\alpha}{2\pi}\;4\alpha(1-\alpha) \quad (36)$$
$$\times\left\{\frac{p_a^x p_a^y}{p_a^2}\left(1+\frac{m}{p_a^2}\ln\left[\frac{p_a^2-m}{-m}\right]\right)\right.$$
$$\left.-\;\frac{p_b^x p_b^y}{p_b^2}\left(1+\frac{m}{p_b^2}\ln\left[\frac{p_b^2-m}{-m}\right]\right)\right\}$$
$$\Phi_{\mathrm{TT}}^{(-+)}(q,k,l) = -\Phi_{\mathrm{TT}}^{(+-)}(q,k,l)\,, \quad (37)$$

with $(p^x, p^y) = \mathbf{p}$. For the helicity conserving parts in the massless quark limit the remaining α integration was also performed analytically and is presented in the appendix. For the result with massive quarks a numerical integration has been performed.

In the same way one can calculate the scattering of real photons into longitudinal Z bosons and obtain (in the $m_f \to 0$ limit):

$$\Phi_{\mathrm{TL}}^{(i)}(q,k,l)$$
$$= \alpha_{\mathrm{s}}\sqrt{N_c^2-1}\sum_f C_f\,2\sqrt{4\pi}\,M_Z\int_0^1\frac{\mathrm{d}\alpha}{2\pi}$$
$$\times\,\alpha(1-\alpha)(1-2\alpha) \quad (38)$$
$$\times\left\{\frac{\boldsymbol{\epsilon}_i\cdot\mathbf{p}_b}{p_b^2}\ln\left[\frac{p_b^2-m}{-m}\right] - \frac{\boldsymbol{\epsilon}_i\cdot\mathbf{p}_a}{p_a^2}\ln\left[\frac{p_a^2-m}{-m}\right]\right\}.$$

In order to compute the two-gluon or the BFKL amplitude one has to substitute these expressions into (1) or (20) and (24).

5 Numerical results

In this section we present numerical results on the QCD corrections for ZZ pair production in $\gamma\gamma$ collisions. Here we consider full circular polarization of the incoming photons. The relative QCD contributions are presented for transverse Z bosons only, because in the high-energy approximation the helicity changing parts of the electroweak amplitude are supressed by powers of s and thus are negligible. Nevertheless we shall display the helicity changing part of the BFKL amplitude as the pure QCD contribution alone. The parameters $\alpha_{\mathrm{W}} = \alpha/s_{\mathrm{W}}^2$, $\alpha = 1/128$, $m_Z = 91.2\,\mathrm{GeV}$, $m_t = 174.3\,\mathrm{GeV}$ and $\alpha_{\mathrm{s}}(s_0)$ have been used throughout the numerical computations. We have been neglecting all quark masses apart from the top quark mass in the numerical calculation, since they are neglible compared to the Z boson mass. The inclusion of the top quark mass reduces the QCD amplitude by 25%.

In terms of the amplitudes (30), (21) and (26) the cross section reads

$$\frac{\mathrm{d}\sigma}{\mathrm{d}p_{\mathrm{T}}^2} = \frac{1}{16\pi s^2}|A_{\mathrm{EW}} + A_{\mathrm{QCD}}|^2\,, \quad (39)$$

where $p_{\mathrm{T}} = |2\,\mathbf{l}|$ is the exchanged transverse momentum. The angular distribution of the cross section is obtained by the relation

$$\mathrm{d}t = \frac{s}{2}\beta\;\mathrm{d}\cos\theta\,, \quad (40)$$

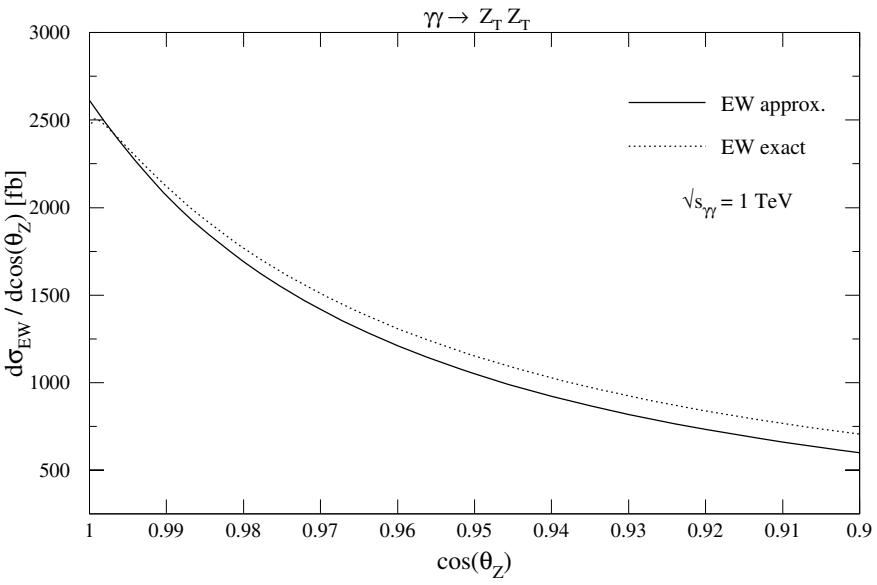

Fig. 4. Angular distribution of the leading electroweak contribution for transverse Z pair production in polarized $\gamma\gamma$ collision at $\sqrt{s} = 1\,\mathrm{TeV}$. The solid line is the result of the high-energy approximation, the dotted line is the result of the exact calculation

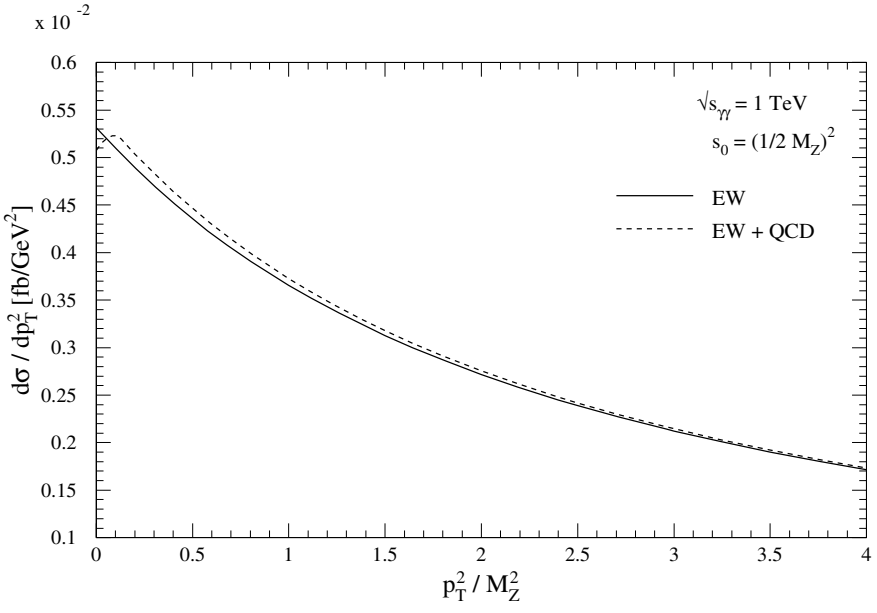

Fig. 5. The pure EW differential cross section (solid line) versus the exchanged transverse momenta at $\sqrt{s} = 1\,\mathrm{TeV}$ and the one which include the QCD corrections (dashed line). For the BFKL contribution the scale $s_0 = (1/2M_Z)^2$ was used

with $\beta = \sqrt{1 - 4M_Z^2/s}$. For small scattering angles in the high-energy approximation the two incoming and two outgoing particles do not "communicate" with each other because of the huge separation in rapidity. As a result, the amplitude with the helicity $++ \to ++$ is equal to the amplitude with helicity $+- \to +-$ etc. Since the helicity conserving amplitudes completely dominate the cross section, after the summation of outgoing helicities the result is the same for all the possibilities of incoming helicities, i.e. $++ \to \mathrm{TT}$ is equal to $+- \to \mathrm{TT}$ etc. In the following $\gamma\gamma \to Z_\mathrm{T} Z_\mathrm{T}$ stands for all these possibilities as well as for unpolarized scattering.

In Fig. 4 the angular distribution of the leading electroweak contribution for transverse Z pair production for polarized $\gamma\gamma$ collision at $\sqrt{s_{\gamma\gamma}} = 1\,\mathrm{TeV}$ is given. The solid line is the result of the calculation in the high-energy approximation, presented in Sect. 4.1. The dotted line is the result of the exact calculation, presented also in [10] for $\sqrt{s_{\gamma\gamma}} = 500\,\mathrm{GeV}$. For $\cos\theta \approx 0.9$ the result of the high-energy approximation has a deviation of $\sim 15\%$ from the exact calculation; for smaller scattering angles the deviation is decreasing. With increasing center of mass energy the accuracy of the Regge calculation is continously increasing.

Let us consider the QCD corrections. In the Born analysis, from the naive counting of the couplings (see Fig. 1), one expects in the interference term a suppression, with respect to the one loop EW case, due to the factor α_s^2 and an additional suppression of a factor ≈ 4 due to the difference in the EW couplings. This would lead to corrections of less than a percent. At high energies in the Regge limit we expect an enhancement due to the appearance of some large logarithms, which may be resummed in the BFKL scheme. We stress that the resummed lead-

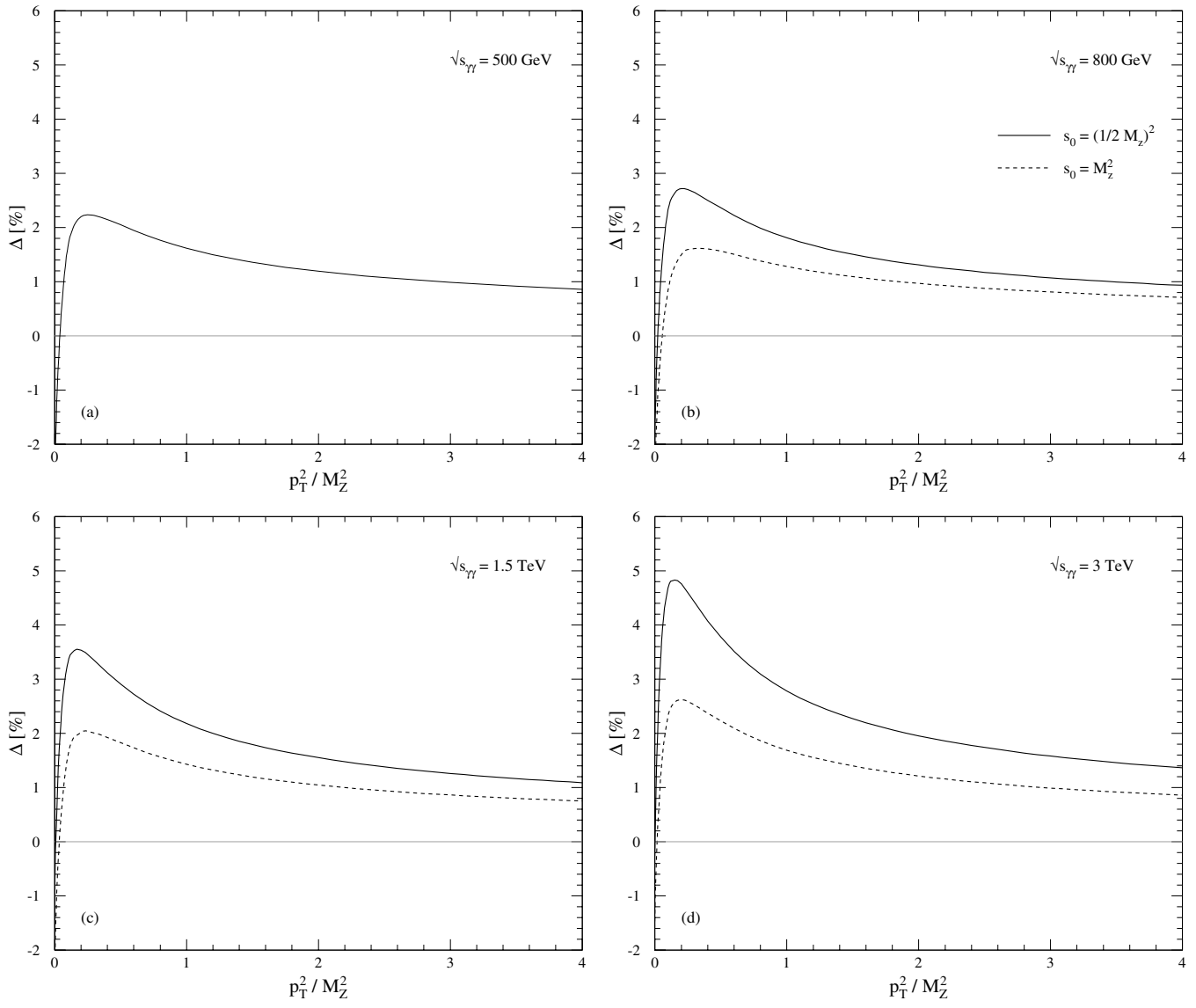

Fig. 6. QCD corrections to the differential cross section relative to the pure EW contribution for different scales s_0 and center of mass energies $\sqrt{s}$. The relative correction is defined as $\Delta = \left(\frac{\mathrm{d}\sigma_{\mathrm{QCD+EW}}}{\mathrm{d}p_{\mathrm{T}}^2} - \frac{\mathrm{d}\sigma_{\mathrm{EW}}}{\mathrm{d}p_{\mathrm{T}}^2}\right) \Big/ \frac{\mathrm{d}\sigma_{\mathrm{EW}}}{\mathrm{d}p_{\mathrm{T}}^2}$

ing log QCD corrections at the lower energies we consider are overshooting what is expected from the real contribution; nevertheless they provide a first estimate. We remind the reader, as discussed previously, that the BFKL resummation is evaluated in the saddle point approximation. Figure 5 displays the differential cross section with respect to the exchanged transverse momenta at a center of mass energy of $\sqrt{s_{\gamma\gamma}} = 1\,\mathrm{TeV}$. The solid line is the pure electroweak cross section, and the dashed line is the one with the QCD corrections included, (39). The cross section has a slight increase approaching the forward region. This slight rise comes from the electroweak part since it completely dominates the amplitude. As in the following will become clear, for the QCD part of the cross section the rise approaching the forward region is much stronger. Therefore the QCD corrections are enhanced close to the forward region.

This behavior is shown in Fig. 6, where the QCD corrections to the differential cross section relative to the pure electroweak contribution at center of mass energies of 500 GeV (a), 800 GeV (b), 1.5 TeV (c) and 3 TeV (d) are shown as functions of p_{T}^2/M_Z^2. At these energies $p_{\mathrm{T}}^2/M_Z^2 = 4$ corresponds to values of $\cos\theta$ (where θ is the scattering angle) of 0.75 (a), 0.90 (b), 0.97 (c) and 0.99 (d) respectively. This relative correction is defined as

$$\Delta = \left(\frac{\mathrm{d}\sigma_{\mathrm{QCD+EW}}}{\mathrm{d}p_{\mathrm{T}}^2} - \frac{\mathrm{d}\sigma_{\mathrm{EW}}}{\mathrm{d}p_{\mathrm{T}}^2}\right) \Big/ \frac{\mathrm{d}\sigma_{\mathrm{EW}}}{\mathrm{d}p_{\mathrm{T}}^2} \ . \qquad (41)$$

Since for leading order BFKL the scale is not fixed, there is an uncertainty which affects the magnitude of the QCD corrections. The solid lines in Fig. 6 are results for the scale $s_0 = (1/2\ M_Z)^2$ while the dashed lines correspond to $s_0 = M_Z^2$. At the scale $s_0 = M_Z^2$ the minimal center of mass energy $\sqrt{s}$, for which the saddle point approximation

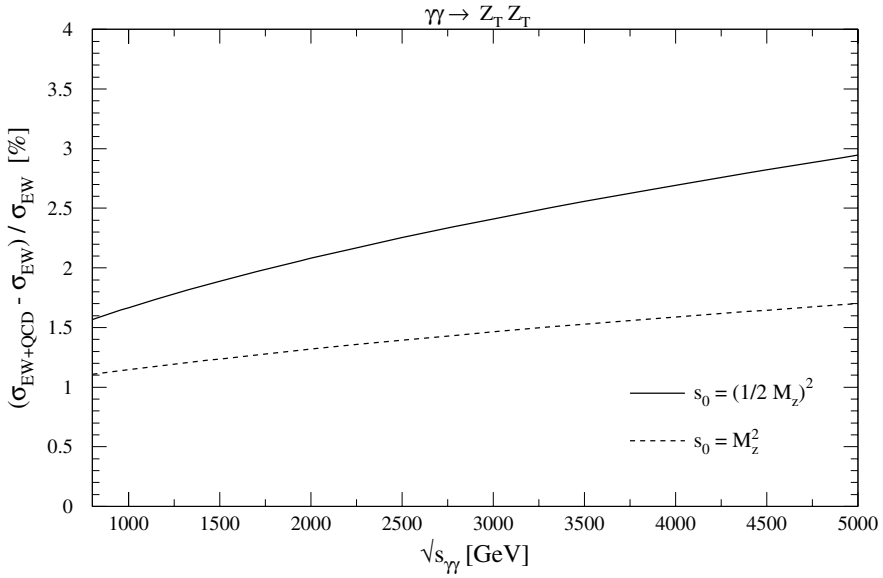

Fig. 7. The QCD corrections to the integrated cross section relative to the pure EW contribution for different scales. The integration region was choosen as $1/4\,M_Z^2 < p_{\mathrm{T}} < 4\,M_Z^2$

for the leading logarithmic calculations gives a reliable result, is 800 GeV. Corrections resulting from leading order BFKL contribution are at the percent level. For higher p_{T} they are about one percent and approaching the forward region (smaller p_{T} values) they rise and lead to corrections of a few percent. Close to the forward region the sign of the corrections is changing as a result of the fact that for small $\mathbf{l}$ the imaginary part of Φ_h (see (20)) gets an enhancement. Figure 6a–d summarizes the dependences of the corrections resulting from leading order BFKL calculations with respect to the center of mass energy $\sqrt{s}$, the exchanged transverse momenta p_{T} and the scale s_0. For rising center of mass energy the corrections increase. The solid lines ($s_0 = (1/2\ M_Z)^2$) in Fig. 6a,d show that the corrections may increase in this regime by a factor of 2 if the energy increases from 500 GeV to 3 TeV. The scale s_0 implicates also a strong dependence. In fact close to the forward region the corrections also grow by a factor of 2 if the scale is decreasing from $s_0 = M_Z^2$ to $s_0 = (1/2\ M_Z)^2$. The biggest dependence is coming from the exchanged momenta or equivalently from the scattering angle. The corrections have a strong increase with decreasing scattering angle or p_{T} and change sign close to the forward region.

In Fig. 7 relative corrections to the integrated cross section $(\sigma_{\mathrm{EW+QCD}} - \sigma_{\mathrm{EW}})/\sigma_{\mathrm{EW}}$ are plotted as a function of the center of mass energy. These are also at the order of percent level. The corrections rise with increasing center of mass energy. The magnitude of the corrections is again scale dependent and the increase is stronger for smaller scales, as expected. Since the calculations are done in the Regge limit we integrated (39) in the region of $1/4\,M_Z^2 < p_{\mathrm{T}} < 4\,M_Z^2$. An integration down to $p_{\mathrm{T}} = 0$ would change the result by less than 0.1%, since the sign of the corrections changes very close to the forward region (see Fig. 6).

If one integrates over all scattering angles the corrections become less important, but since the main contribution of the cross section is coming from small scattering angles the result would not be affected strongly.

In the following figures some properties of the pure QCD part of the amplitude are discussed. In Fig. 8 the absolute value of the QCD amplitudes is displayed for the helicity conserving case.

The solid line is the BFKL (resummed) contribution while the dashed line is the Born (two-gluon) contribution. At $\sqrt{s} = 1\,\mathrm{TeV}$ the gluon resummation is enhancing the pure QCD Born amplitude by one order of magnitude. The same enhancement is visible in the QCD corrections to the electroweak cross section. Both amplitudes are increasing with decreasing p_{T}, whereas for higher energies the rise of the resummed amplitude will be stronger as the Born one.

In Fig. 9 the absolute value of the two helicity changing parts of the amplitude at $\sqrt{s} = 1\mathrm{TeV}$ are plotted. The most noticable property is that the helicity changing parts are suppressed by more than two orders of magnitude with respect to the helicity conserving part. The $++ \to --$ cross section has, apart from its magnitude, properties similar to $++ \to ++$, for example its slope as a function of p_{T}. The $++ \to \mathrm{LL}$ part is also rising when p_{T} is getting smaller but in the region of $p_{\mathrm{T}} = 1/2\,M_Z$ it has an extremum and is steeply going to zero for $p_{\mathrm{T}} = 0$. This behavior comes from (9), where the integrand is antisymmetric in $\alpha \leftrightarrow (1-\alpha)$ for $\mathbf{l} = 0$.

6 Conclusions

In this paper we have presented formulae for the leading QCD corrections to vector boson scattering at small scattering angles. These emerge since, like the photon, all vector bosons fluctuate into quark–antiquark pairs, which are strongly interacting color dipoles. The non-forward boson impact factors describe the probability that the boson fluctuates into a quark–antiquark dipole. First the Born and after the leading logarithmic resummed (BFKL) con-

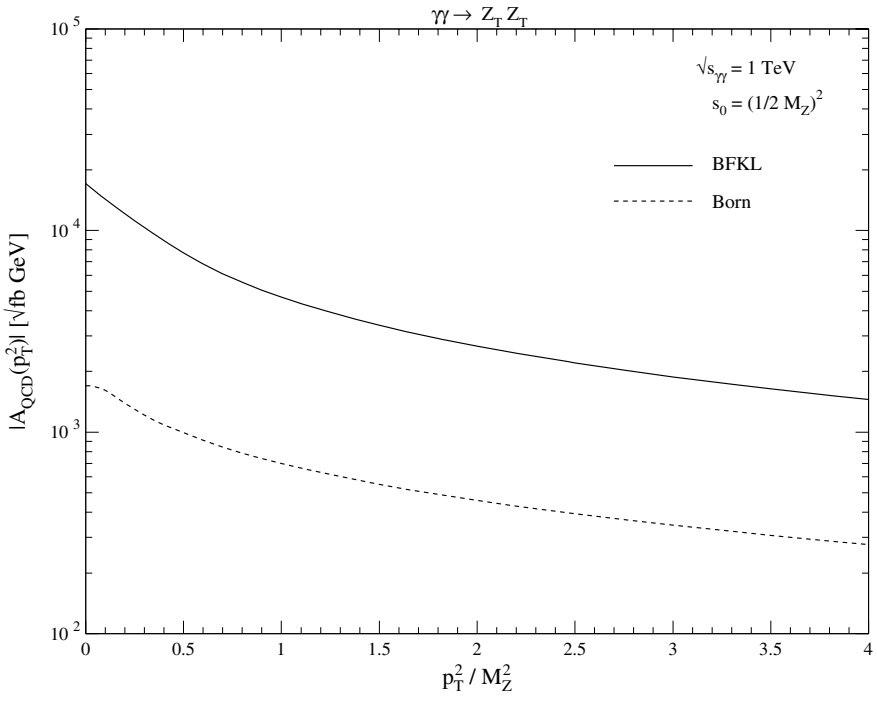

Fig. 8. The pure QCD part of the amplitude versus the exchanged transverse momenta. The solid line is the BFKL contribution and the dashed line is the QCD Born approximation (two-gluon amplitude)

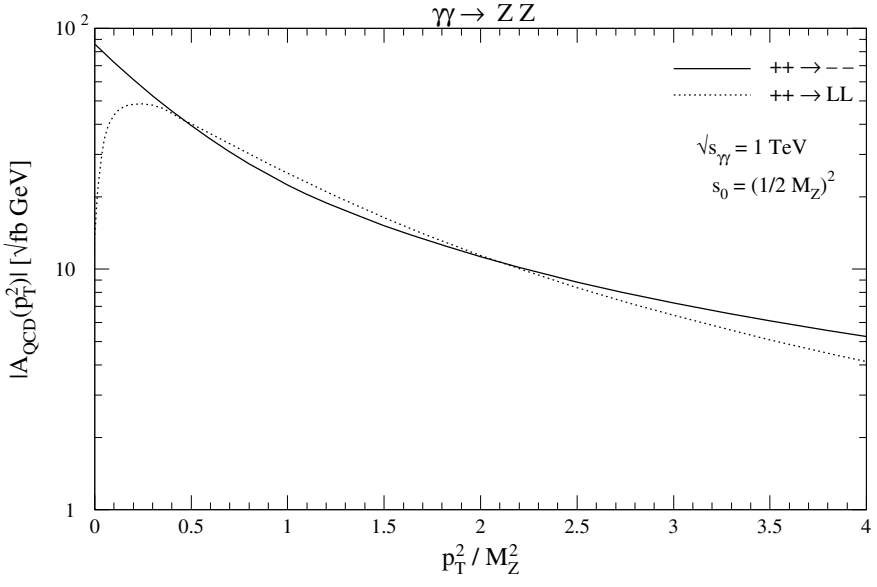

Fig. 9. The same as Fig. 8 for the helicity changing parts of the BFKL contribution

tributions have been investigated for an arbitrary process of elastic scattering of vector bosons.

In particular the process $\gamma\gamma \to ZZ$ has been considered in detail. Both, the electroweak and the QCD parts of the amplitude have been calculated in the high-energy approximation. The results are displayed for the differential and integrated cross section, comparing QCD corrections relative to the one loop electroweak calculation. We discussed some properties of the pure QCD part of the cross section as well, including also non-leading contributions. The general result of the numerical calculation is that at $s = O(1\,\mathrm{TeV})$ the QCD corrections affect the cross section of the process by a few percents. The corrections are smaller for larger p_T values and rise with falling p_T. Moreover they rise with the center of mass energy, as expected. Since the leading log BFKL contribution ends up with a noticable scale dependence this results should not be regarded as a precision calculation. Therefore, we interpret this result as an indication that, in particular in the small angle region, possible deviations from EW calculations cannot be interpreted as signals of new physics without taking into account the QCD corrections.

The same reasoning is valid for the integrated cross sections, since the biggest contribution to the cross section is coming from scattering at small angles.

Acknowledgements. We wish to thank J. Bartels for many helpful discussions. Furthermore we wish to thank G.

Chachamis for giving us data regarding exact EW calculations, and S. Dittmaier for helpful discussions. K.P. is supported by the Graduiertenkolleg "Zukünftige Entwicklungen in der Teilchenphysik". G.P. Vacca thanks J. Bartels and the II. Institut für Theoretische Physik for the warm hospitality.

Appendix

In this appendix we present further formulas for the impact factor calculated in Sect. 4.2.

In the case of massive fermions (34) has the form

$$\begin{aligned}
&\Phi_{\mathrm{TT}}^{(++)}(q,k,l)\\
&= \alpha_{\mathrm{s}}\sqrt{N_c^2-1}\sum_f C_f\,\frac{1}{\sqrt{\pi}}\int_0^1 \mathrm{d}\alpha\left\{[\alpha^2+(1-\alpha)^2]\right.\\
&\times\left[\frac{p_a^2-m+2\,m_f^2}{2\,\Delta_a}\left(\log\left[\frac{-m-p_a^2-\Delta_a}{-m-p_a^2+\Delta_a}\right]\right.\right.\\
&\qquad\left.-\log\left[\frac{-m+p_a^2-\Delta_a}{-m+p_a^2+\Delta_a}\right]\right)\\
&-\frac{p_b^2-m+2\,m_f^2}{2\,\Delta_b}\left(\log\left[\frac{-m-p_b^2-\Delta_b}{-m-p_b^2+\Delta_b}\right]\right.\\
&\qquad\left.\left.-\log\left[\frac{-m+p_b^2-\Delta_b}{-m+p_b^2+\Delta_b}\right]\right)\right]\\
&-\frac{m_f^2}{\Delta_a}\left(\log\left[\frac{-m-p_a^2-\Delta_a}{-m-p_a^2+\Delta_a}\right]-\log\left[\frac{-m+p_a^2-\Delta_a}{-m+p_a^2+\Delta_a}\right]\right)\\
&\left.+\frac{m_f^2}{\Delta_b}\left(\log\left[\frac{-m-p_b^2-\Delta_b}{-m-p_b^2+\Delta_b}\right]-\log\left[\frac{-m+p_b^2-\Delta_b}{-m+p_b^2+\Delta_b}\right]\right)\right\},
\end{aligned}\tag{42}$$

while (38) becomes

$$\begin{aligned}
&\Phi_{\mathrm{TL}}^{(i)}(q,k,l)\\
&= \alpha_{\mathrm{s}}\sqrt{N_c^2-1}\sum_f C_f\,\frac{2}{\sqrt{\pi}}M_Z\int_0^1 \mathrm{d}\alpha\,\{\alpha(1-\alpha)(1-2\alpha)\\
&\times\left[\frac{\boldsymbol{\epsilon}_i\cdot\mathbf{p}_b}{2\,p_b^2}\left(\frac{p_b^2-m}{\Delta_b}\left(\log\left[\frac{-m-p_b^2-\Delta_b}{-m-p_b^2+\Delta_b}\right]\right.\right.\right.\\
&\qquad\left.\left.\left.-\log\left[\frac{-m+p_b^2-\Delta_b}{-m+p_b^2+\Delta_b}\right]-\log\left[\frac{m_f^2-m}{m_f^2}\right]\right)\right)\right]\\
&-\left[\frac{\boldsymbol{\epsilon}_i\cdot\mathbf{p}_a}{2\,p_a^2}\left(\frac{p_a^2-m}{\Delta_a}\left(\log\left[\frac{-m-p_a^2-\Delta_a}{-m-p_a^2+\Delta_a}\right]\right.\right.\right.\\
&\qquad\left.\left.\left.-\log\left[\frac{-m+p_a^2-\Delta_a}{-m+p_a^2+\Delta_a}\right]-\log\left[\frac{m_f^2-m}{m_f^2}\right]\right)\right)\right],
\end{aligned}\tag{43}$$

with

$$\begin{aligned}
\Delta_a &= \sqrt{(p_a^2-m)^2+4m_f^2\,p_a^2}\,,\\
\Delta_b &= \sqrt{(p_b^2-m)^2+4m_f^2\,p_b^2}\,,
\end{aligned}\tag{44}$$

and p_a^2, p_b^2 and m was already defined in Sect. 4.2. Taking the limit $m_f\to 0$ one obtains (34) and (38) respectively. This formulas were used for the top quark contribution, where the remaining α integration was done numerically.

In the case of massless fermions for the helicity conserving part the α integration may be performed analytically, giving the result

$$\begin{aligned}
&\Phi_{\mathrm{TT}}^{(++)}(q,k,l)\\
&= \alpha_{\mathrm{s}}\sqrt{N_c^2-1}\sum_f C_f\,\frac{1}{\sqrt{\pi}}\left\{2\left(x_1-x_1^2+x_2-x_2^2\right)\right.\\
&+\left(2-3\,x_1+3\,x_1^2-2\,x_1^3\right)\log(1-x_1)\\
&+\left(3\,x_1-3\,x_1^2+2\,x_1^3\right)\log(-x_1)\\
&+\left(2-3\,x_2+3\,x_2^2-2\,x_2^3\right)\log(1-x_2)\\
&+\left(3\,x_2-3\,x_2^2+2\,x_2^3\right)\log(-x_2)\\
&+\frac{1}{3a^3}\left[d\,\left(-3\,a^2+3\,a\,d+2\,d^2\right)\,\log\left(\frac{d}{a}\right)\right.\\
&\left.\left.+\,(a+d)\left(2ad-\left(2a^2+ad+2d^2\right)\,\log\left(1+\frac{d}{a}\right)\right)\right]\right\},
\end{aligned}\tag{45}$$

with

$$\begin{aligned}
a &= 4\,\mathbf{l}^2+M_Z^2+\mathrm{i}\epsilon\,,\\
b &= -4(\mathbf{l}^2+\mathbf{kl})-M_Z^2-\mathrm{i}\epsilon\,,\\
c &= (\mathbf{k}+\mathbf{l})^2,\\
d &= -M_Z^2-\mathrm{i}\epsilon\,,\\
x_{1,2} &= \frac{-b\pm\sqrt{b^2-4ac}}{2a}\,.
\end{aligned}\tag{46}$$

References

1. M. Baillargeon, G. Belanger, F. Boudjema, hep-ph/9405359
2. B.W. Lee, C. Quigg, H.B. Thacker, Phys. Rev. D **16**, 1519 (1977)
3. G. Bélanger, F. Boudjema, Phys. Lett. B **288**, 210 (1992); K.A. Peterson, S. Godfrey, hep-ph/9302297; O.J.P. Éobli, M.C. Gonzaléz-García, S.F. Novaes, Nucl. Phys. B **411**, 381 (1994), hep-ph/9306306; O.J.P. Éobli, M.B. Magro, P.G. Mercandante, S.F. Novaes, Phys. Rev. D **52**, 15 (1995), hep-ph/9503432; S. Godfrey, hep-ph/9505252; G.J. Gounaris, F.M. Renard, Z. Phys. C **69**, 513 (1996), hep-ph/9505429; G.J. Gounaris, J. Layssac, F.M. Renard, Z. Phys. C **69**, 505 (1996), hep-ph/9505430; M. Baillargeon, G. Bélanger, F. Boudjema, Nucl. Phys. B **500**, 224 (1997), hep-ph/9701372; E. Boos et al., hep-ph/0103090
4. F. Boudjema, in Physics and Experiments with Linear e^+e^- Colliders, Waikoloa, Hawaii, 1993, edited by F.A. Harris et al. (World Scientific), vol. II, p. 712
5. G.J. Gounaris, J. Layssac, P.I. Porfyriadis, F.M. Renard, Eur. Phys. J. C **13**, 79 (2000)
6. J.L. Hewett, F.J. Petriello, Phys. Rev. D **64**, 095017 (2001)
7. T.G. Rizzo, Phys. Rev. D **60**, 115010 (1999), hep-ph/9904380; K. Cheung, Phys. Rev. D **61**, 015005 (2000), hep-ph/9904266; H. Davoudiasl, Phys. Rev. D **60**, 084022 (1999), hep-ph/9904425; Phys. Rev. D **61**, 044018 (2000), hep-ph/9907347

8. A. Denner, S. Dittmaier, T. Hahn, Phys. Rev. D **56**, 117 (1997); A. Denner, T. Hahn, Nucl. Phys. B **525**, 27 (1998); A. Denner, S. Dittmaier, R. Schuster, Nucl. Phys. B **452**, 80 (1995)
9. E.A. Kuraev, L.N. Lipatov, V.S. Fadin, Sov. Phys. JETP **44**, 443 (1976); **45**, 199 (1977); Ya.Ya. Balitskii, L.N. Lipatov, Sov. J. Nucl. Phys. **28**, 822 (1978)
10. G. Jikia, Nucl. Phys. B **405**, 24 (1993)
11. J. Bartels, K. Golec-Biernat, K. Peters, Acta Phys. Polon. B **34**, 3051 (2003)
12. S.J. Brodsky, F. Hauptmann, D.E. Soper, Phys. Rev. D **56**, 6957 (1997)
13. H. Cheng, T.T. Wu, Phys. Rev. **182**, 1852, 1868, 1873, 1899 (1969)
14. V.S. Fadin, L.N. Lipatov, Phys. Lett B **429**, 127 (1998), and references therein; M. Ciafaloni, G. Camici, Phys. Lett. B **430**, 430 (1998)
15. J. Bartels, M.A. Braun, D. Colferai, G.P. Vacca, Eur. Phys. J. C **20**, 323 (2001), hep-ph/0102221
16. L.N. Lipatov, Pomeron in quantum chromodynamics, in Perturbative QCD, pp. 411–489, edited by A.H. Mueller (World Scientific, Singapore 1989); Phys. Rep. **286**, 131 (1997)
17. J. Bartels, M.G. Ryskin, G.P. Vacca, Eur. Phys. J. C **27**, 101 (2003), hep-ph/0207173